Available online at www.sciencedirect.com
ScienceDirect
Journal of the European Ceramic Society 30 (2010) 2763–2771
www.elsevier.com/locate/jeurceramsoc

# Effect of stoichiometry and milling processes in the synthesis and the piezoelectric properties of modified KNN nanoparticles by solid state reaction

F. Rubio-Marcos [a,*], J.J. Romero [a], M.S. Martín-Gonzalez [b], J.F. Fernández [a]

[a] *Electroceramic Department, Instituto de Cerámica y Vidrio, CSIC, Kelsen 5, 28049 Madrid, Spain*
[b] *Instituto de Microelectrónica de Madrid, CSIC, C/Isaac Newton 8, 28760 Tres Cantos, Madrid, Spain*

Received 21 October 2009; received in revised form 18 May 2010; accepted 29 May 2010
Available online 30 June 2010

**Abstract**

Nanoparticles in the system (K,Na,Li)(Nb,Ta,Sb)$O_3$, modified KNN, were synthesized following a solid state reaction procedure. Milling of the individual carbonate and oxide raw materials was carried out before mixing of the components to optimize particle size. These mixtures were calcined at 700 °C for 2 h, obtaining nanoparticles with size ranging between 50 and 200 nm. The optimization of the raw materials particle size and the particle refinement of the carbonates during their decomposition play a key role in the formation of the modified KNN nanoparticles by solid state route. The obtained nanoparticles show tetragonal and orthorhombic phases coexistence that could be attributed in part to the lack of homogeneity of cations distribution confirmed by EDS analysis. The $K^+$ cation excess on the modified KNN system produces a displacement of $Li^+$ cations from the perovskite structure that is the origin of the stabilization of the orthorhombic symmetry. These nanoparticles are used to sintered ceramics with good piezoelectric properties without needing of anisotropic preparation methods. The sintered ceramics show resistance to hygroscopicity and deliquescence.
Published by Elsevier Ltd.

*Keywords:* (A) Powders-solid state reaction; (B) Microstructure-prefiring (C) Piezoelectric properties; (D) Perovskites

## 1. Introduction

The search for alternative lead-free piezoelectric materials is now being focused on alkali niobate based systems in which a morphotropic phase boundary (MPB) occurs.[1–3] Over the past few years, much attention has been given to the "old" lead-free compound ($Na_{0.5}K_{0.5}$)$NbO_3$ (KNN) because of its good electrical properties.[4] A morphotropic phase boundary (MPB) occurs in KNN and, as for lead titanate–zirconate piezoceramics, PZT, an enhancement of the properties is observed for compositions near to this MPB. However, the major drawbacks of KNN ceramics are (i) the need for special handling of the starting powders due to volatility of alkaline elements, (ii) high sensitivity of the properties to stoichiometry, and (iii) complex densification processes.[5] These problems have been known for a long time and thus, the PZT compounds are preferred for applications due to the reliability of the solid state reaction processes. The alkaline metal elements forming part of the KNN materials easily evaporate at high temperatures and cause compositional fluctuations and poorer properties, as it was well known for the piezoelectric PZT system.[6]

Exceptionally high piezoelectric properties have been previously reported in the system (K,Na)$NbO_3$–$LiTaO_3$–$LiSbO_3$ for ceramics prepared by a complex processing method.[7] Recent studies demonstrated compositional inhomogeneities associated with alkali volatilization and abnormal grain growth for Li/Ta-modified KNN[8,9] which resulted in different properties for the same nominal composition processed by different ways. Therefore, the processing and powder synthesis are critical steps in obtaining such materials. Recently, KNN-based systems have been obtained through "soft chemistry" methods as sol–gel[10] and microemulsion.[11] The use of soft chemistry to prepare nanoparticles should improve the densification and allows a reduction of the synthesis temperature, reducing the volatilization of alkali elements. However, most of the chemical methods could not avoid the appearance of carbonates during the

* Corresponding author. Tel.: +34 91 735 5840; fax: +34 91 735 5843.
*E-mail address:* frmarcos@icv.csic.es (F. Rubio-Marcos).

0955-2219/$ – see front matter. Published by Elsevier Ltd.
doi:10.1016/j.jeurceramsoc.2010.05.027

Table 1
Main characteristic of the reagents used for synthesis of $K_{0.44+x}$NL–NTS by solid state reaction, as well the average particle size, $d_{50}$, of the raw materials before and after the milling stage.

| Raw materials | Commercial reference | Purity (%) | $\rho^{25\,^{\circ}C}$ (g/cm$^3$) | Melting point (°C) | $d_{50}$ (μm) as received | $d_{50}$ (μm) milled | Physical form |
|---|---|---|---|---|---|---|---|
| $Na_2CO_3$ | PANREAC, Montplet & Esteban | >99.5 | 2.54 | 858 | 6.7 | 1.7 | White, monoclinic, hygroscopic |
| $K_2CO_3$ | MERCK. Darmstadt | >99.0 | 2.29 | 898 | 12.8 | 2.3 | White, monoclinic, hygroscopic |
| $Li_2CO_3$ | PANREAC, Montplet & Esteban | >99.5 | 2.11 | 723 | 10.5 | 2.8 | White, monoclinic, |
| $Nb_2O_5$ | SIGMA–ALDRICH CHEMIE | >99.9 | 4.60 | 1512 | 2.1 | 0.6 | White, orthorhombic |
| $Ta_2O_5$ | SIGMA–ALDRICH CHEMIE | >99.0 | 8.20 | 1784 | 10.1 | 1.0 | White, rhombohedric |
| $Sb_2O_5$ | SIGMA–ALDRICH CHEMIE | >99.995 | 4.12 | Decompose at 380 | 15.2 | 3.2 | Yellow, cubic |

thermal treatment and thus high temperatures are finally required to synthesize adequate powders. Solid state reaction routes from oxides and carbonates have been extensively used to synthesize ferroelectric powders with good control of particle morphology. Moreover, solid state reaction synthesis is a low cost technique and requires only simple processing. Thus, this technique would be highly desirable for technological applications.

In this work, we report the synthesis and characterization of $(K_{0.44+x}Na_{0.52}Li_{0.04})(Nb_{0.86}Ta_{0.10}Sb_{0.04})O_3$ ($K_{0.44+x}$NL–NTS) nanopowders produced via solid state reaction. The effects of $K^+$ content on the phase structure, morphology and microstructure of $K_{0.44+x}$NL–NTS nanopowders are studied. In addition the piezoelectric properties of sintered ceramics made from the nanopowders were evaluated.

## 2. Experimental

Ceramic powders with compositions $(K_{0.44+x}Na_{0.52}Li_{0.04})(Nb_{0.86}Ta_{0.10}Sb_{0.04})O_3$, hereafter $K_{0.44+x}$NL–NTS, with $x = -0.06$, $-0.04$, $-0.02$, 0.00, 0.02 and 0.04, were synthesized by conventional solid state reaction. The raw materials used in this study are potassium carbonate ($K_2CO_3$, 99.0%), sodium carbonate ($Na_2CO_3$, 99.5%), lithium carbonate ($Li_2CO_3$, 99.5%), niobium oxide ($Nb_2O_5$, 99.5%), tantalum oxide ($Ta_2O_5$, 99.0%) and antimony oxide ($Sb_2O_5$, 99.995%). In all the experiments, raw materials were dried prior to use at 200 °C for 1 h, because of their hygroscopic nature. Raw materials were milled individually (attrition milling in ethanol for 3 h), in order to obtain an appropriate particle size distribution.[12] Table 1 shows the median particle size, $d_{50}$, of the raw materials before and after the milling stage. The as received materials presented a wide dispersion of particle sizes. The milling process produces a homogenization of the particle sizes, obtaining median particle sizes, $d_{50}$, between 0.6 and 3 μm, for the milled raw materials. These median particle size data were an order of magnitude smaller than the $d_{50}$ value of the as received materials. These powders were then weighed and mixed by attrition milling using $ZrO_2$ balls in ethanol medium for 3 h, dried and calcined at 700 °C for 2 h with a heating rate of 3 °C/min.

The calcined powders were attrition milled again and pressed at 200 MPa into disks of 10 mm in diameter and 0.7 mm in thickness. The pellets were finally sintered in air at 1125 °C for different times, from 1 to 16 h. The density of the sintered samples was measured using the Archimedes method. For the electrical measurements, a fired silver paste was used for the electric contacts. The samples were change by polarized in a silicon oil bath at 25 °C by applying a direct current electric field of 4.0 kV/mm during 30 min.[13]

Simultaneous thermogravimetric and differential thermal analysis were carried out on $K_{0.44+x}$NL–NTS samples before and after the calcination step using a NETZSCH STA 409 analyzer. Around 50 mg of powder was placed in a Pt/Rh crucible and heated up to 1200 °C with a heating rate of 3 °C/min. The measurements were performed in a flowing air atmosphere.

The infrared spectra were recorded using a Perkin-Elmer FTIR 1720X spectrometer. A few milligrams of the sample were mixed with KBr in an agate mortar, disk pressed and recorded from 4000 to 400 cm$^{-1}$. The infrared bands of interest were located between 400 and 1800 cm$^{-1}$. The crystalline symmetry was determined by X-ray diffraction analysis (XRD, Siemens D5000, Munich, Germany, Cu $K_\alpha$ radiation). The lattice parameters of the sintered ceramics were refined by a method of global simulation of the full diagram using the pattern matching routine of fullprof program.

The particle size and morphology were evaluated using field emission scanning electron microscopy, FE-SEM (Hitachi S-4700, Tokio, Japan), equipped with energy dispersive spectroscopy, EDS, and transmission electron microscopy (TEM, Philips CM 200 FEGTEM, Eindhoven, Netherlands) with an accelerating voltage of 200 kV. For TEM investigations, powders were suspended in isopropanol, and a drop of this suspension was deposited on a holey carbon-coated film supported on a 400 mesh copper grid. Surface area measurements were performed using a 3-point BET technique (Quantachrome Instruments, Florida, USA).

The Raman scattering was measured in air atmosphere and at room temperature, by using 488 nm radiation from an $Ar^+$ laser operating at 10 mW. The signal was collected by a microscope Raman spectrometer (Renishaw Micro-Raman System 1000) in the 100–3000 cm$^{-1}$ range.

The piezoelectric constant $d_{33}$ was measured using a piezo-$d_{33}$ meter (YE2730A $d_{33}$ METER, APC International, Ltd., USA). The electromechanical coupling factor $k_p$ was determined at room temperature by resonance and antiresonance methods on the basis of IEEE standards.

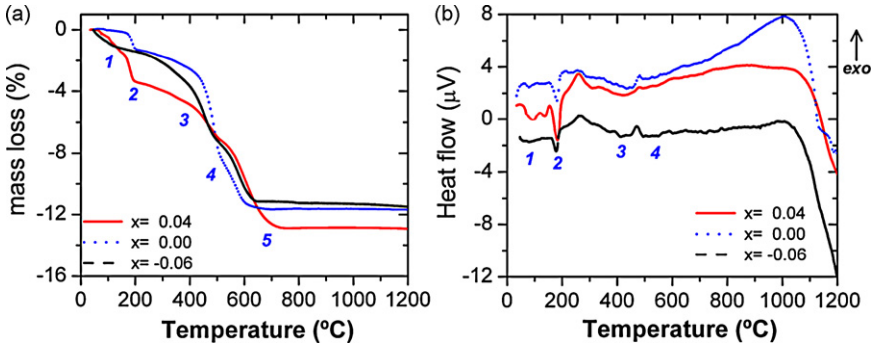


Fig. 1. TG (a) and DTA (b) curves of the $K_{0.44+x}$NL–NTS mixtures.

## 3. Results and discussion

Fig. 1 shows the results of the TG/DTA for the $K_{0.44+x}$NL–NTS mixtures. The samples experiment a mass loss between 11.1 and 12.7% upon heating to 700 °C. The highest mass loss was recorded for over-stoichiometric samples, $x = 0.04$. Four weight loss peaks can be observed on the TG curve, Fig. 1a, at 80, 180, 345 and 480 °C, associated with endothermic peaks, Fig. 1b. The first weight loss occurring at 80 °C is attributed to the removal of absorbed environmental moisture water. The sub-stoichiometric and stoichiometric compositions, $-0.06 \leq x \leq 0.00$, show ~0.5% weight loss on this process, meanwhile the potassium rich composition, $x \geq 0.04$ shows bigger weight loss. The weight loss peak at 180 °C is related to simultaneous losses of $H_2O$ and $CO_2$.[14] The decomposition of $AHCO_3$ to $A_2CO_3$, where A is $K^+$, $Na^+$ or $Li^+$, occurs between 100 and 180 °C.[15] According with these data, it would mean that 1.6 wt% of $AHCO_3$ is formed after the ethanol milling step from the $H_2O$ and $CO_2$ present in the atmosphere. The endothermic peaks at 345 and 480 °C are consistent with the polymorphic transition of $A_2CO_3$.[16] The main weight losses occurred in a narrow temperature range between 400 and 690 °C, corresponding to the $CO_2$ losses. At temperatures above 700 °C, the decomposition of carbonates has been completed. For compositions between $-0.06 \leq x \leq 0.00$, the complete decomposition temperature is similar and occurs at ~600 °C, while for $x \geq 0.04$ the required temperature to finish the complete carbonate decomposition is ~700 °C. Based on these results, the optimum calcination treatment was selected at 700 °C during 2 h.

Fig. 2a and b show FTIR studies of the $K_{0.44+x}$NL–NTS mixtures and calcined $K_{0.44+x}$NL–NTS powders on the region between 1800 and 400 $cm^{-1}$. The IR spectra of the initial mixtures, Fig. 2a, show four main absorption bands at ~1640, ~1460 $cm^{-1}$ (double peak), 880 and 630 $cm^{-1}$. The weak absorption band at 1640 $cm^{-1}$ can be attributed to the in-plane bending vibration of $H_2O$.[19] The band at ~1460 $cm^{-1}$ can be assigned to the C–O asymmetrical stretching ($\upsilon_3$) and the group of bands at ~ 880 $cm^{-1}$ to the $CO_3^{2-}$ out-of-plane deformation ($\upsilon_2$) of the carbonate group.[15] The broad band appearing at 630 $cm^{-1}$ could be ascribed to the characteristic vibration of B–O, where B is $Nb^{+5}$, $Ta^{+5}$ and $Sb^{+5}$ cations.

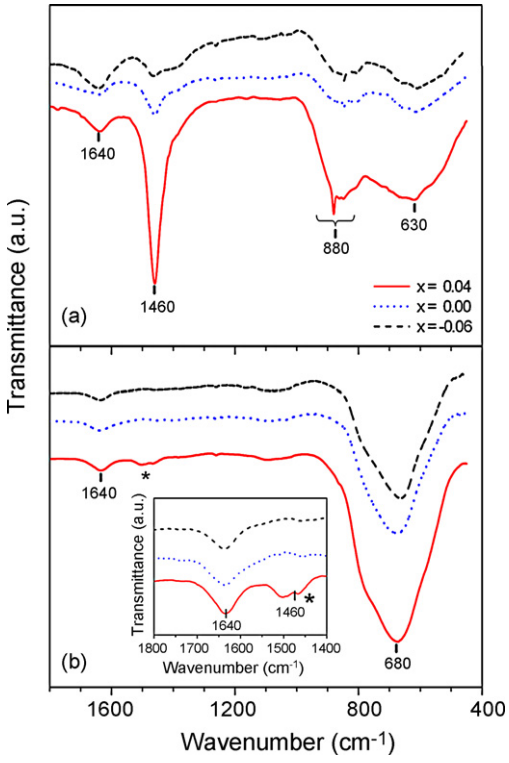


Fig. 2. FTIR plots of the (a) $K_{0.44+x}$NL–NTS mixtures and (b) calcined $K_{0.44+x}$NL–NTS powders as a function of the composition. The inset shows a detail of the region between 1800 and 1400 $cm^{-1}$.

The IR spectra of the calcined $K_{0.44+x}$NL–NTS powders, Fig. 2b, show a complete disappearance of the absorption band at 1460 $cm^{-1}$, ascribed to vibrations of the $CO_3^{2-}$ group, for sub-stoichiometric and stoichiometric compositions, $-0.06 \leq x \leq 0.00$. Meanwhile, in the over-stoichiometric samples this band is still present, as shown in the inset of Fig. 2b. The broad strong band centered at 680 $cm^{-1}$ indicates the formation of the perovskite phase.[17] These results are in good agreement with the ones observed by TG/DTA, where the weight losses corresponding to decomposition of carbonates were completed at ~700 °C.

The calcined $K_{0.44+x}$NL–NTS powders consist of agglomerates 300–500 nm in size, which are formed by smaller plate-like particles in the range 50–150 nm depending on the composition, Fig. 3. The obtention of nanopowders by the solid state reaction

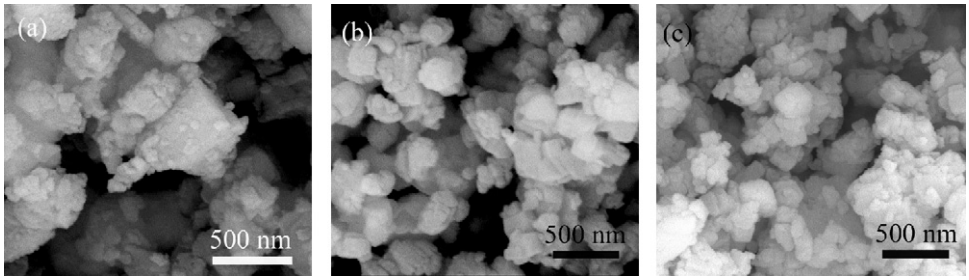


Fig. 3. FE-SEM photographs of the calcined $K_{0.44+x}$NL–NTS powders: (a) $x = -0.06$, (b) $x = 0.00$ and (c) $x = 0.04$.

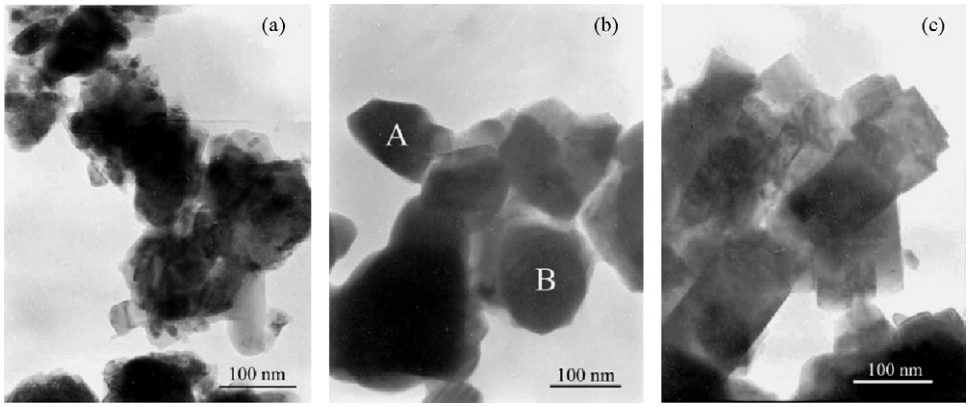


Fig. 4. TEM photographs of the $K_{0.44+x}$NL–NTS powders calcined at 700 °C during 2 h as a function of the composition: (a) $x = -0.06$, (b) $x = 0.00$ and (c) $x = 0.04$.

procedure is attributed to the decomposition reaction from carbonates to oxides, which may be responsible for the refinement of the particle size.[18,19]

TEM micrographs of the calcined $K_{0.44+x}$NL–NTS powders reveal in detail the nanopowders morphology, Fig. 4. The nanoparticles are comparable in size with those obtained by "soft chemistry" methods.[10,11] The sub-stoichiometric samples show strongly agglomerated particles with acicular morphology and particle size <100 nm, Fig. 4a. The stoichiometric powders show nearly spherical like particles as well as a few platelet particles with sizes ranged 100–150 nm, Fig. 4b. Finally, the over-stoichiometric powders are formed by particles with platelet morphology that correspond to nearly rectangular particles. The platelets possess a lateral size <200 nm and a considerably lower thickness, Fig. 4c. As the amount of starting $K_2CO_3$ increases, the nanoparticles evolve from small acicular nanoparticles to nearly rectangular platelets having larger size along the plane dimensions than the spherical like particle of lower stoichiometry. BET measurements showed a specific surface area ~9.7 $m^2/g$ for sub-stoichiometric nanopowders and 9.5 $m^2/g$ for stoichiometric and over-stoichiometric nanopowders. These high BET values are comparable with those obtained by "soft chemistry" methods[10,11] and are in agreement with the nanoparticles dimension of the synthesized powders.

X-ray diffraction (XRD) patterns of the calcined powders show main peaks that can be easily associated to the KNN perovskite structure, together with minor secondary phases identified as $Ta_2O_5$ for the sub-stoichiometric samples, Fig. 5a. The presence of $Ta_2O_5$ remnants from the starting mixtures was related to the lower reactivity of $Ta_2O_5$ compared to $Nb_2O_5$.[20] The main phase of the sub-stoichiometric samples can be well related to a tetragonal perovskite phase, whereas for the over-stoichiometric samples the XRD pattern presents features that can be associated to phase coexistence between tetragonal and orthorhombic perovskite phases,[21] although the broadening of the peaks made it difficult to fully resolve the peaks corresponding to any individual crystalline symmetry.

The crystallite size of the nanopowders was calculated from the full width at half maximum of the diffraction peaks using the Scherrer's equation (after correction of the data by the instrumental broadening of the system):

$$D = \frac{k \times \lambda}{B \times \cos\theta}$$

where $D$ is the crystallite size, $\lambda$ is the X-ray wavelength, $B$ is the full width at half maximum of the diffraction line, $\theta$ is the angle of diffraction and $k$ is a constant (~0.9). Fig. 5c shows the evolution of the crystallite size as a function of the composition. The size increases form $26 \pm 7$ nm for sub-stoichiometric samples to $46 \pm 23$ nm for over-stoichiometric ones. Both the average crystallite size and the dispersion of the crystalline size (error bars correspond to the standard deviation) increase almost linearly with the presence of $K^+$ in the composition, in good agreement with the trend observed by TEM (Fig. 4). The particle size observed by TEM are larger than the ones calculated by XRD, indicating that each particle is composed of different coherent crystalline regions.

The different reactivity between $Nb_2O_5$ and $Ta_2O_5$ observed by XRD was corroborated by EDS analysis of the calcined $K_{0.44}$NL–NTS powder particles. Fig. 6a shows the EDS anal-

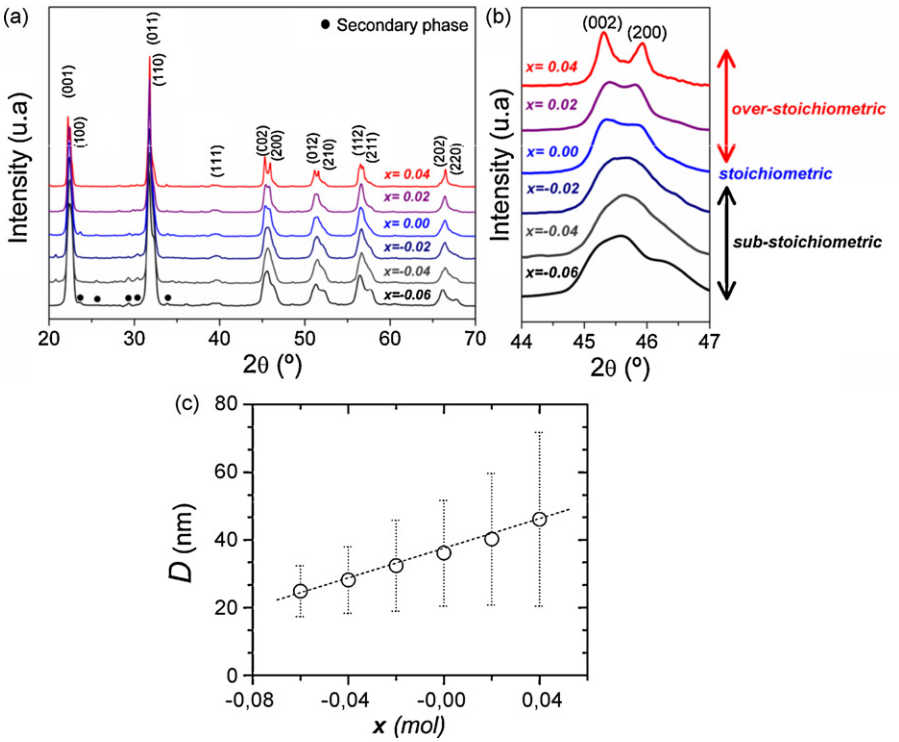


Fig. 5. (a) XRD patterns of the $K_{0.44+x}NL$–NTS powders of the different composition calcined for 2 h at 700 °C, where $x$ varied between −0.06 and 0.04 and (b) detail of the 2$\theta$ region from 44° to 47°. (c) Evolution of the crystallite size as a function of the composition.

ysis of a $Ta^{5+}$ rich particle marked as A in Fig. 4b. The EDS microanalysis shows very high levels of $Ta_2O_5$ indicating a low reactivity. On the other hand, particles with nominal composition are commonly observed, Fig. 6b, where the EDS analysis of the particle marked as B in Fig. 4b is shown. The observation of $Ta^{5+}$ rich particles indicates the existence of compositional heterogeneities in the nanopowders.

The Raman spectra of the calcined nanopowders are shown in Fig. 7. The main vibrations are associated to the $BO_6$ perovskite-octahedra.[22] The vibrations of the $BO_6$ octahedron consist of $1A_{1g}$ ($\upsilon_1$) + $1E_g$ ($\upsilon_2$) + $2F_{1u}$ ($\upsilon_3$, $\upsilon_4$) + $F_{2g}$ ($\upsilon_5$) + $F_{2u}$ ($\upsilon_6$). Of these vibrations, $1A_{1g}$ ($\upsilon_1$) + $1E_g$ ($\upsilon_2$) + $1F_{1u}$ ($\upsilon_3$) are stretching modes and the rest are bending modes. In particular, $A_{1g}$ ($\upsilon_1$) and $F_{2g}$ ($\upsilon_5$) are detected as relatively strong scatterings in systems similar to the one we are studying, because of a near-perfect equilateral octahedral symmetry. All the calcined samples were confirmed as consisting of a perovskite phase. For over-stoichiometric sample, minor bands at high wave number region can be assigned to the residual carbonate phases. Furthermore, we should not exclude from the discussion the fact that the O–H stretch of $H_2O$ appears near 2650 $cm^{-1}$, which can eventually overlap with hydrogen carbonate bands.[23]

A detail of the region between 440 and 760 $cm^{-1}$ is presented in Fig. 8a, where the spectrum is fitted to the sum of two Lorentzian functions centered at ~555 and ~615 $cm^{-1}$, ascribed to Eg ($\upsilon_2$) and $A_{1g}$ ($\upsilon_1$) Raman modes, respectively, according to the literature.[22] The $A_{1g}$ ($\upsilon_1$) peak shifts to lower frequencies when the amount of $K^+$ cations increases (see Fig. 8b) due to a decrease in the strength constant caused by the lengthening of the distance between $B^{5+}$ type ions and their coordinated

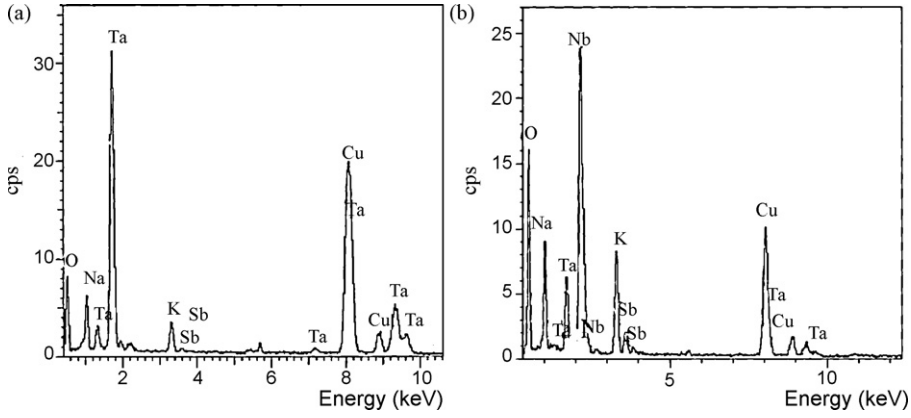


Fig. 6. EDS spectra of (a) a $Ta^{5+}$ rich particle and (b) a particle with nominal composition, corresponding to the ones marked as A and B, respectively, in Fig. 4b.

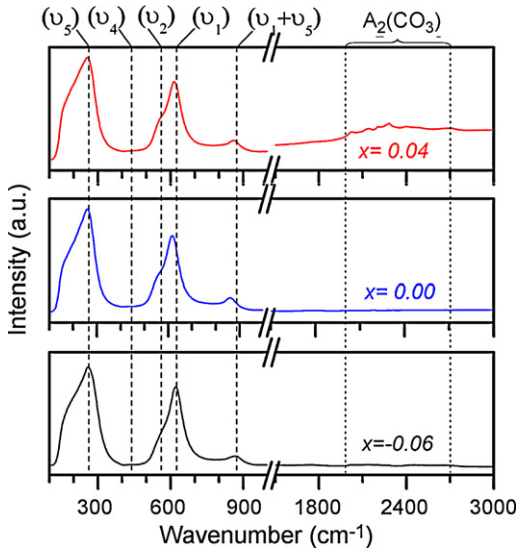


Fig. 7. Raman spectra of calcined $K_{0.44+x}$NL–NTS powders depending on the composition: $x = -0.06$, $x = 0.00$ and $x = 0.04$.

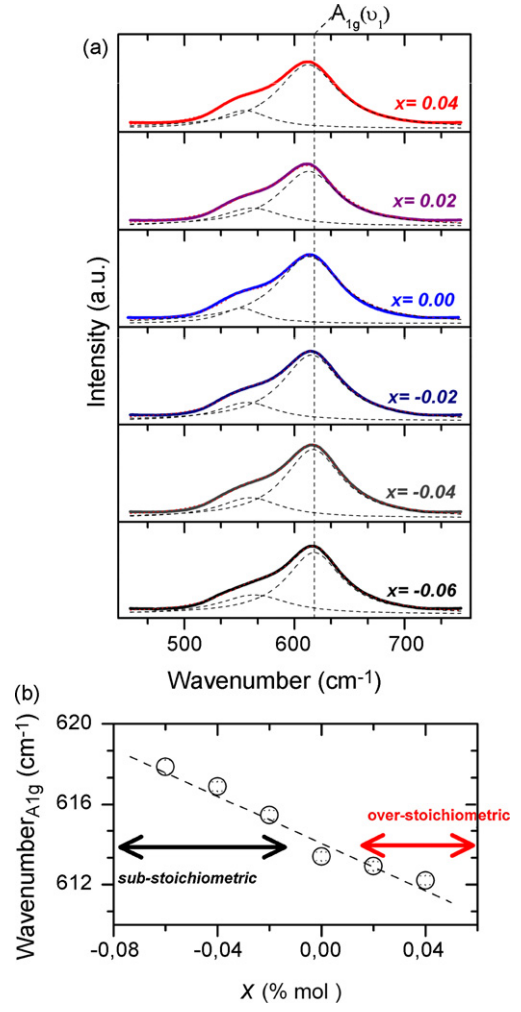


Fig. 8. (a) Magnified Raman spectra in the wave number ranges from 440 to 760 $cm^{-1}$ as function of the composition and Lorentzian fits of the individual peaks of the Eg ($\upsilon_2$) and $A_{1g}$ ($\upsilon_1$) Raman modes. (b) Evolution of the Raman shift of $A_{1g}$ modes as a function of the composition.

oxygens. This type of position shift has been previously associated in sintered ceramics with an evolution from tetragonal to orthorhombic phase.[21] Taking this into account, it can be said that in the sub-stoichiometric samples, the tetragonal symmetry is dominant at room temperature, as previously inferred from the XRD results, whereas for the over-stoichiometric samples the structure evolves towards an orthorhombic symmetry. This indicates that the structure tends to orthorhombic simmetry when the $K_2CO_3$ content increases.

In KNLN and related systems, the orthorhombic to tetragonal phase transition shifts towards lower temperatures when the concentration of $Li^+$ cations increases.[22,24] The $Li^+$ cations compete with $Na^+$ and $K^+$ in the A sites of $ABO_3$ perovskite to form a solid solution. The structure of the solid solution transforms from orthorhombic to tetragonal symmetry due to the large distortion caused by the incorporation of $Li^+$ cations.[22,25] This may be attributed to the smaller ionic radius of $Li^+$ compared to $Na^+$ and $K^+$.[25] This stabilization of the orthorhombic symmetry at room temperature with the increasing of $K^+$ concentration has been observed in our samples by Raman spectroscopy. This behaviour could be associated with an excess of $K^+$ cations in the $K_{0.44+x}$NL–NTS system which causes a displacement of $Li^+$ cations from the perovskite structure and therefore the stabilization of the orthorhombic symmetry phase.

The nanopowders obtained have been used for the production of ceramic samples by a simple sintering process in air at 1125 °C for different times, from 1 to 16 h. Sintering in open air is the most suitable method for industrial mass production of ceramic samples. All the obtained ceramics show relative densities over 95% of the theoretical value (see Table 2). This demonstrates that the use of the nanopowder precursor allows the production of well sintered ceramics of modified KNN. Moreover, no relevant weight losses have been observed during the sintering, indicating that there are no alkaline materials volatilization.

Table 2 summarizes typical data of sintering density, grain size, crystal symmetry (including the presence of secondary phases) and tetragonality ratio (c/a, obtained from the fitting of the full XRD pattern with the fullprof program) of $K_{0.44+x}$NL–NTS ceramics as a function of the stoichiometry, for sintering times of 1 and 16 h. For all compositions the bulk density slightly increases with increasing sintering time. This evolution agrees well with the one reported for $LiTaO_3$-modified KNN, for which an increase of the densities was observed for sintering times up to ≈10 h.[8]

The average grain size increases slightly with sintering time. The sub-stoichiometric samples show a greater grain size than the stoichiometric and the over-stoichiometric ones, as can be observed on the micrographs presented in Fig. 9 for samples sintered for 16 h. This behaviour has been reported in our previous works concerning Li/Ta/Sb modified KNN piezoelectric ceramics with composition $(K_{0.44+x}Na_{0.52}Li_{0.04})(Nb_{0.86}Ta_{0.10}Sb_{0.04})O_3$[21,26] demonstrating that K deficiency (and thus excess $B^{+5}$ cations) improved the sinterability compared to stoichiometric compositions. For the K-deficient compositions, the densification occurs via a liquid phase that promotes grain growth, but induces the occurrence of a secondary phase of tetragonal tungsten bronze structure

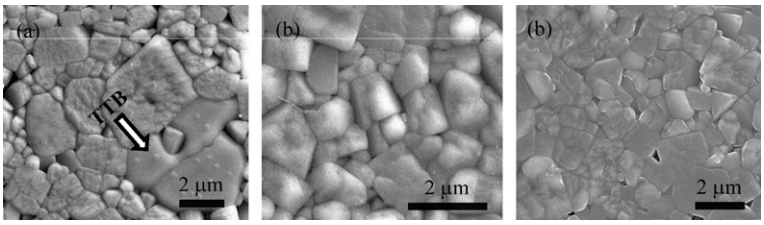


Fig. 9. Micrographs of samples sintered for 16 h prepared with: (a) sub-stoichiometric, (b) stoichiometric and (c) over-stoichiometric nanopowders. In figure (c) the presence of a grain with TTB structure is signalled.

(TTB),[26] see Fig. 9a, similar to the one observed for $LiTaO_3$ and $LiNbO_3$-modified KNN. The quantity of this secondary phase decreases with sintering time. Previous studies devoted to modified KNN[8,9] also evidenced the presence of abnormal grains, with cylindrical morphology and very large dimensions, which are not observed here. This fact indicates that the EDS observed compositional heterogeneities are compensated by the high reactivity of nanopowders.

The sintered samples present the coexistence of tetragonal and orthorhombic phases at room temperature due to a phase polymorphism[21,27] (see Table 2). The tetragonal symmetry is the main phase on the sub-stoichiometric ceramics and evolves to orthorhombic symmetry for the over-stoichiometric ceramics, for sintering time 1 h, in close relation with the main phase present on the starting nanoparticles. The increasing of sintering time enhances the c/a ratio of the tetragonal phase, in all cases. These data are in agreement with a recent work[28] that established the increasing of the tetragonality ratio, c/a, on modified KNN systems with the $Li^+$ content. Then, the observed increase of the c/a ratio could indicate an increase of $Li^+$ incorporation in the perovskite structure with the sintering time.

These results suggest that the starting nanoparticles composition affects the structure of the sintered ceramics and thus its properties. The preparation of the nanopowders causes an improvement on the sinterability and better compositional homogenization due to reduction of the diffusion distance of the concerned elements as previously suggested by Wang et al.[8] Furthermore, this process inhibits the abnormal grain growth, and stabilization of the tetragonal symmetry at room temperature in the KNL–NTS system.

The remanent polarization (Pr) of the $K_{0.44+x}$NL–NTS sintered ceramics for different values of $x$ and sintering times are summarized in Table 2. The sub-stoichiometric and stoichiometric ceramics show well saturated hysteresis loops and large values of Pr ($\sim$18.5 μC/cm$^2$), especially for high sintering times (16 h). However, the over-stoichiometric ceramics present lower Pr values and for 1 h sintered samples the presence of conduction effects. The piezoelectric properties previously established for the KNL–NTS system, show a linear evolution of the $d_{33}$ values with the tetragonality ratio: the higher the tetragonality ratio of the system the higher their piezoelectric properties are.[21,29] This same trend is observed also in the present results (see Table 2). This linear dependence was associated to the stabilization of the tetragonal phase at room temperature in expense of the orthorhombic one, i.e., the decrease of the polymorphism phase transition temperature.[21,29] Therefore, the stoichiometry

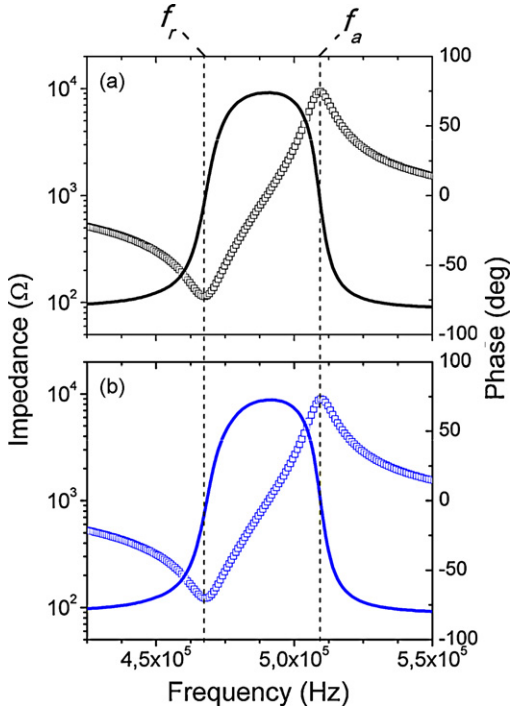


Fig. 10. Resonance and antiresonance spectra of $K_{0.44}$NL–NTS sintered ceramics at 1125 °C for 16 h before (a) and after being exposed to water (b).

of the KNL–NTS system, which must be controlled in the early stages, plays an important role in the stabilization of the different crystalline symmetries and on their piezoelectric properties.

Some studies devoted to KNN-based ceramics also demonstrated that these materials present sintering difficulties and exhibit deliquescence[30] and formation of hygroscopic secondary products[31] when they are exposed to moisture. We have immersed KNN-based ceramics of this work in water for a long time (48 h), observing no hygroscopicity or deliquescence behaviour. Fig. 10 shows typical data on the frequency dependence of phase and impedance for $K_{0.44+x}$NL–NTS piezoceramics sintered at 1125 °C for 16 h before and after 48-h immersion in water. No differences were observed between the piezoelectric resonance and antiresonance, confirming that the $K_{0.44+x}$NL–NTS sintered ceramics are free from hygroscopicity or deliquescence problems.

Therefore, the KNL–NTS nanopowders prepared by solid state reaction and sintered in an air atmosphere have the potential to be among the leading lead-free piezoceramic materials in the future.

Table 2
Several properties and typical electrical properties of $K_{0.44+x}$NL–NTS ceramics sintered at 1125 °C. T*: tetragonal symmetry, O*: orthorhombic symmetry (tetragonal P4*nm* and orthorhombic *Amm*2). TTB***: a minor secondary phase detected by DRX which was assigned to $K_3LiNb_6O_{17}$ (PDF#36-0533), with tetragonal tungsten–bronze structure.[21,26].

| Composition | Sintering time (h) | Density (g/cm$^3$) ±0.01 | Density relative to theoric (%) | Grain size (μm) | Cristal phase | Secondary phase TTB*** (%) | tetragonality ratio (c/a) ±0.0001 | $P_r$ (μC/cm$^2$) | $d_{33}$ (pC/N) |
|---|---|---|---|---|---|---|---|---|---|
| Sub-stoichiometric ($x = -0.06$) | 1 | 4.61 | 96.6 | 1.4 ± 0.8 | T* | 3.5 ± 0.2 | 1.0093 | 15.0 ± 1.0 | 148 ± 10 |
| | 16 | 4.69 | 98.3 | 1.7 ± 1.0 | T* | 1.2 ± 0.1 | 1.0108 | 17.5 ± 1.0 | 230 ± 15 |
| Stoichiometric ($x = 0.00$) | 1 | 4.64 | 97.3 | 0.6 ± 0.4 | O** + T* | – | 1.0071 | 5.9 ± 0.5 | 57 ± 5 |
| | 16 | 4.70 | 98.5 | 1.2 ± 0.6 | T* | – | 1.0110 | 18.5 ± 1.5 | 255 ± 15 |
| Over-stoichiometric ($x = 0.04$) | 1 | 4.74 | 99.4 | 0.6 ± 0.4 | O** | – | – | – | 40 ± 5 |
| | 16 | 4.76 | 99.8 | 1.3 ± 0.7 | O** + T* | – | 1.0079 | 10.0 ± 2.0 | 102 ± 6 |

## 4. Conclusion

A method to produce modified KNN nanoparticles by solid state reaction process has been developed. The nanoparticles obtained varied from 50 to 200 nm as a function of the stoichiometry. X-ray diffraction and Raman spectroscopy showed an orthorhombic symmetry stabilization when the concentration of alkaline cations increased. The excess of $K^+$ cations in the $K_{0.44+x}$NL–NTS system may cause a displacement of $Li^+$ cations from the perovskite structure. Therefore, the stoichiometry of the KNL–NTS system plays an important role in the stabilization of the crystalline symmetries and thus on their related piezoelectric properties. The stabilization of the tetragonal crystalline symmetries produces an improvement of the piezoelectric properties in comparison to the samples where the orthorhombic phase is present. The sintered samples showed an improvement on the sinterability, inhibition of abnormal grain growth, stabilization of the tetragonal symmetry and are free from hygroscopicity or deliquescence behaviour when compared with previously reported materials.

## Acknowledgments

The authors express their thanks to the CICYT projects MAT2007-66845-C02-01 and to the MAGIN project PIF2006-60f0121 for their financial support. Dr. F. Rubio-Marcos thanks the FPI-CAM-FSE program for the research grant. Dr. J.J. Romero is indebted to CSIC for a "Junta de Ampliación de Estudios" contract (ref. JAEDOC087).

## References

1. Guo Y, Kikuta K, Hirano S. Piezoelectric properties of $(K_{0.5}Na_{0.5})(Nb_{1-x}Ta_x)O_3{}^-K_{5.4}CuTa_{10}O_{29}$ ceramics. *J Appl Phys* 2005;**97**:114105.
2. Zuo RZ, Fang XS, Ye C. Phase structures and electrical properties of new lead-free $(Na_{0.5}K_{0.5})NbO_3$–$(Bi_{0.5}Na_{0.5})TiO_3$ ceramics. *Appl Phys Lett* 2007;**90**(art. no.):092904.
3. Wu J, Xiao D, Wang Y, Zhu J, Yu P, Jiang Y. Compositional dependence of phase structure and electrical properties in $(K_{0.42}Na_{0.58})NbO_3$–$LiSbO_3$ lead-free ceramics. *J Appl Phys* 2007;**102**(art. no.):114113.
4. Egerton L, Dillon DM. Piezoelectric and dielectric properties of ceramics in the system potassium–sodium niobate. *J Am Ceram Soc* 1959;**42**:438–42.
5. Matsubara M, Yamaguchi T, Sakamoto W, Kikuta K, Yogo T, Hirano S. Processing and piezoelectric properties of lead-free (K,Na) $(NbTa)O_3$ ceramics. *J Am Ceram Soc* 2005;**88**:1190–6.
6. Fernandez JF, Moure C, Villegas M, Durán P, Kosec M, Drazic G. Compositional fluctuations and properties of fine-grained acceptor-doped PZT ceramics. *J Eur Ceram Soc* 1998;**18**:1695–705.
7. Saito Y, Takao H, Tani T, Nonoyama T, Takatori K, Homma T, et al. Lead-free piezoceramics. *Nature (London)* 2004;**432**:84–7.
8. Wang Y, Damjanovic D, Klein N, Hollenstein E, Setter N. Compositional inhomogeneity in Li- and Ta-modified (K, Na)$NbO_3$ ceramics. *J Am Ceram Soc* 2007;**90**:3485–9.
9. Wang Y, Damjanovic D, Klein N, Setter N. High-temperature instability of Li- and Ta-modified (K,Na)$NbO_3$ piezoceramics. *J Am Ceram Soc* 2008;**91**:1962–70.
10. Chowdhury A, Bould J, Zhang Y, James C, Milne SJ. Nano-powders of $Na_{0.5}K_{0.5}NbO_3$ made by a sol–gel method. *J Nanopart Res*; doi:10.1007/s11051-009-9595-0.

11. Pithan C, Shiratori Y, Dornseiffer J, Haegel F-H, Magrez A, Waser R. Microemulsion mediated synthesis of nanocrystalline $(K_x,Na_{1-x})NbO_3$ powders. *J Cryst Growth* 2005;**280**:191–200.
12. Rubio-Marcos F, Ochoa P, Fernandez JF. Sintering and properties of lead-free (K,NaLi)(Nb,Ta,Sb)$O_3$ ceramics. *J Eur Ceram Soc* 2007;**27**:4125–9.
13. Rubio-Marcos F, Romero JJ, Ochoa DA, García JE, Perez R, Fernández JF. Effects of poling process on KNN-modified piezoceramic properties. *J Am Ceram Soc* 2010;**93**:318–21.
14. Rojac T, Kosec M, Šegedin P, Malič B, Holc J. The formation of a carbonate complex during the mechanochemical treatment of a $Na_2CO_3$–$Nb_2O_5$ mixture. *Solid State Ionics* 2006;**177**:2987–95.
15. Heda PK, Dollimore D, Alexander KS, Chen D, Law E, Bicknell P. A method of assessing solid state reactivity illustrated by thermal decomposition experiments on sodium bicarbonate. *Thermochim Acta* 1995;**255**:255–72.
16. Harris MJ, Salje EKH. The incommensurate phase of sodium carbonate: an infrared absorption study. *J Phys Condens Matter* 1992;**4**:4399–408.
17. Wang C, Hou Y, Ge H, Zhu M, Wang H, Yan H. Sol–gel and characterization of lead-free LNKN nanocrystalline powder. *J Cryst Growth* 2008;**310**:4635–9.
18. Yuhua Zhen, Jing-Feng Li. Normal sintering of (K,Na)$NbO_3$-based ceramics: influence of sintering temperature on densification, microstructure, and electrical properties. *J Am Ceram Soc* 2006;**89**:3669–75.
19. Vela E, Peiteado M, García F, Caballero AC, Fernández JF. Sintering behaviour of steatite materials with barium carbonates flux. *Ceram Int* 2007;**33**:1325–9.
20. Palatnikov MN, Sidorov NV, Kalinnikov VT. Solid-state reactions in the system $Li_2CO_3$–$Na_2CO_3$–$Nb_2O_5$–$Nb_2O_5$. *Inorg Mater* 2008;**44**:750–5.
21. Rubio-Marcos F, Navarro-Rojero MG, Romero JJ, Marchet P, Fernandez JF. Piezoceramic properties as a function of the structure in the system (K, Na, Li)(Nb, Ta, Sb)$O_3$. *IEEE Trans Ultrason Ferroelectric Freq contr* 2009;**56**(9):1835–42.
22. Kakimoto K, Akao K, Guo Y, Ohsato H. Raman scattering study of piezoelectric $(Na_{0.5}K_{0.5})NbO_3$–$LiNbO_3$ ceramics. *Jpn J Appl Phys* 2005;**44**:7064–7.
23. Davis AR, Oliver BG. A vibrational-spectroscopic study of the species present in $CO_2$–$H_2O$ system. *J Solution Chem* 1974;**1**(4):329–39.
24. Klein N, Hollenstein E, Damjanovic D, Trodahl HJ, Setter N, Kuball M. A study of the phase diagram of (K,Na,Li)$NbO_3$ determined by dielectric and piezoelectric measurements, and Raman spectroscopy. *J Appl Phys* 2007;**102**(art. no.):014112.
25. Lin D, Kwok KW, Lam KH, Chan HLW. Structure and electrical properties of $K_{0.5}Na_{0.5}NbO_3$–$LiSbO_3$ lead-free piezoelectric ceramics. *J Appl Phys* 2007;**101**(art. no.):074111.
26. Rubio-Marcos F, Marchet P, Merle-Méjean T, Fernández JF. Role of sintering time, crystalline phases and symmetry in the piezoelectric properties of lead-free KNN- modified ceramics (Li/Na/K)(Nb/Ta/Sb)$O_3$. *Mat Chem Phys* 2010;**123**:91–7.
27. Ochoa DA, García JA, Pérez R, Gomis V, Albareda A, Rubio-Marcos F, et al. Extrinsic contributions and nonlinear response in lead-free KNN-modified piezoceramics. *J Phys D: Appl Phys* 2009;**42**(art. no.):025402.
28. Sun X, Deng J, Chen J, Sun C, Xing X. Effects of Li substitution on the structure and ferroelectricity of (Na,K)$NbO_3$. *J Am Ceram Soc* 2009;**92**:3033–6.
29. Rubio-Marcos F, Navarro-Rojero MG, Romero JJ, Fernández JF. Effect of ZnO on the structure, microstructure and electrical properties of KNN-modified piezoceramics. *J Eur Ceram Soc* 2009;**29**:3045–52.
30. Kakimoto K, Masuda I, Ohsato H. Lead-free $KNbO_3$ piezoceramics synthesized by pressure-less sintering. *J Eur Ceram Soc* 2005;**25**:2719–22.
31. Kosec M, Kolar D. On activated sintering and electrical properties of $NaKNbO_3$. *Mater Res Bull* 1975;**50**:335–40.